# Nonlinear Metrology and Quantum Chaos

*Sashank Kaushik, IIT Madras*

## 1 Introduction

Nitrogen Vacancy Centers are spin-1 defects in diamonds that have become prime candidates for nanoscale MRI, magnetic sensing, single-photon sources, quantum metrology, and quantum-enhanced measurement, as well as quantum repeaters and quantum memory devices. They serve as sensitive probes to measure magnetic fields and temperature. NV-centers provide a rich avenue to explore multi-parameter estimation (for example, the simultaneous measurement of temperature and magnetic field in a single experiment). At a more fundamental level, this project focuses on exploiting non-classical and non-linear dynamics, with NV-centers, to achieve better sensitivity of measurements, and also study the fundamental connection between quantum chaos and decoherence. It involves understanding the chaotic dynamics arising out of the non-linear terms in the NV-centre Hamiltonian and how they connect to the generalised picture of Non-linear Metrology from [1]. Chaotic dynamics of quantum systems has shown promise in quantum metrology as a means to beat the Standard Quantum Limit (SQL) by providing an exponential sensitivity to parameters that the system encodes, as shown in [3]. On the other hand, quantum metrology with Many-body Hamiltonians that have coupling interactions have shown proven lower bounds on the minimum uncertainty of the parameter beyond even the Heisenberg limit (HL) which is usually achievable via entanglement or squeezing in a linear Hamiltonian. The project's efforts focus on exploring this connection between Quantum Chaos and Non-linear metrology and ascertaining if the hypothesised lower bounds can be achieved with the KT Hamiltonian.

### 1.1 Overview

The report will cover broadly 3 parts:

1. *Dynamics of the NV-center spin*: We will explore the spin dynamics of the NV-center under the effect of magnetic fields along the NV-axis and perpendicular to it, including the effect of relaxation processes.
2. *The Kicked-Top Hamiltonian of a Superradiant spin ensemble*: With the introduction of the KT Hamiltonian, we will explore the scaling of the Quantum Fisher Information, an important metric in quantum metrology, with the evolution time and the system size.
3. *The KT Hamiltonian from a Non-linear Metrology perspective*: Finally, we will establish the mathematical lower bounds on the QFI for a general many-body Hamiltonian and validate it for the KT Hamiltonian with simulations to support our findings.

All of the simulation data for this work has been generated using the QuTip library [5].

## 2 Modelling the NV-center

We first simulate the NV-center spin dynamics to assess its capabilities as a good two-level system and its behaviour under different pulse sequences and decay rates. The NV-center Hamiltonian is

quite complex, consisting of two orbital levels between the valence band and conduction band of the crystal, with corresponding fine and hyperfine splittings under different conditions. For the purpose of qubit dynamics, the spin Hamiltonian of the orbital ground state subspace is analyzed.

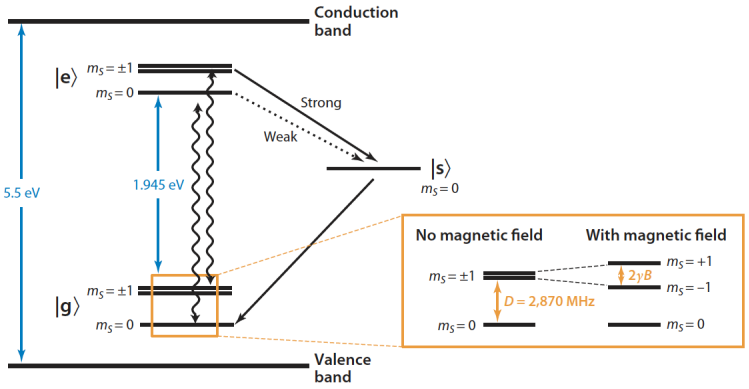


Fig. 1: Energy-level diagram of $NV^-$, as given in [6]

The spin Hamiltonian, from [6], is given by:

$$\frac{\mathcal{H}}{\hbar} = D\left(S_z^2 - \frac{2}{3}\right) + \gamma \mathbf{B}\cdot\mathbf{S} + \epsilon_z E_z\left(S_z^2 - \frac{2}{3}\right) + \epsilon_{xy}\{E_x(S_xS_y + S_yS_x) + E_y(S_x^2 + S_y^2)\} \tag{1}$$

where the first term is the zero-field splitting and the second term is the Zeeman interaction, while the rest are electric field and strain interactions. For this section, we consider only the zfs and Zeeman terms.

## 2.1 Spin-1/2 Rabi Dynamics

Initially, the Spin-$\frac{1}{2}$ modelling is done with the standard Spin Hamiltonian and the external fields inducing Rabi oscillation. We also add relaxation effects (both $T_1$ and $T_2$) to the dynamics. Data is collected for different initial basis states and superpositions and plots are generated using the data from the list of expectation values to show spin dynamics with a) No pulses (Larmor precession) b) $\pi$-pulse ($R_x(\pi)$ gate) c) $\frac{\pi}{2}$-pulse ($R_x(\frac{\pi}{2})$ gate). $T_2^*$ decay can also be added via free evolution decay and Lindblad operators to run spin echo simulations.

## 2.2 Spin-1 Rabi Dynamics

Spin-1 resonance is modelled by spanning a larger subspace and including the zero-field splitting, thereby allowing us to select the transitions via the microwave frequency. The field magnitudes are taken in the millitesla range while maintaining the difference in scaling of ∼100 between B0 and B1, keeping the ZFS as the dominant interaction as per the experimental setup. Simulations are run with different initial states, this time setting the microwave frequency to either of the resonances given by $D + \omega_0$ or $D - \omega_0$, allowing a selection of the transitions from the $m_s = 0$ state to $m_s = +1$ or $m_s = -1$. Plots are generated for both the spin operator expectation values as well as the transition probabilities for both resonance frequencies, showing all the three cases of spin dynamics as done for spin-$f\frac{1}{2}$.

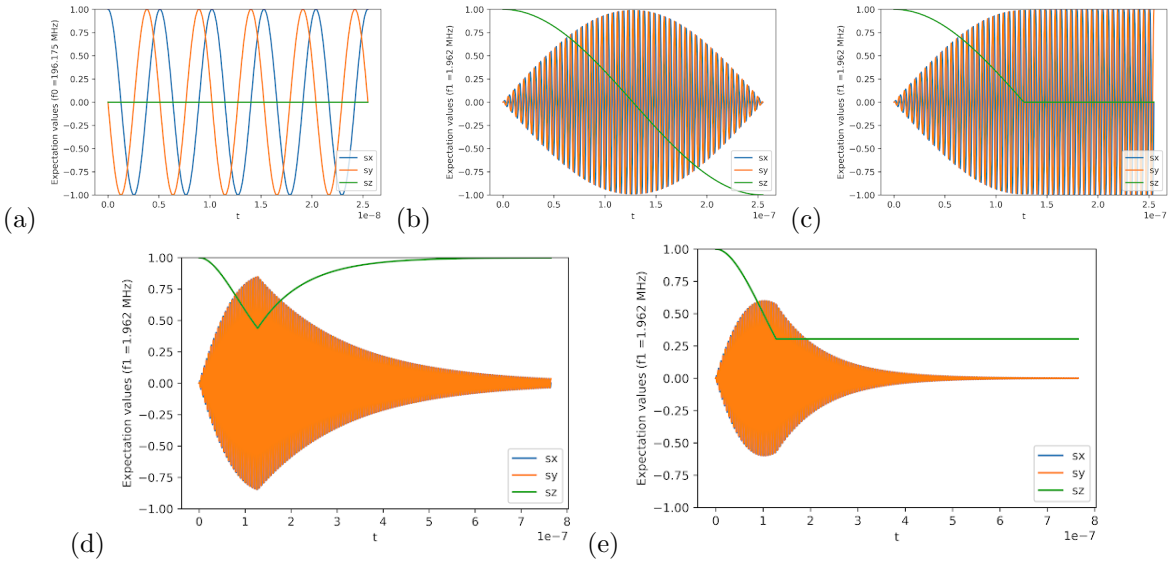


Fig. 2: (a) Larmor precession of the spin-$\frac{1}{2}$ qubit on the equator of the Bloch sphere under a constant axial magnetic field, (b) Application of a $\pi$-pulse on the qubit in the $|0\rangle$ state, (c) Application of a $\frac{\pi}{2}$-pulse on the qubit in the $|0\rangle$ state, (d) & (e) Application of a $\frac{\pi}{2}$-pulse under $T_1$ and $T_2$ relaxation respectively.

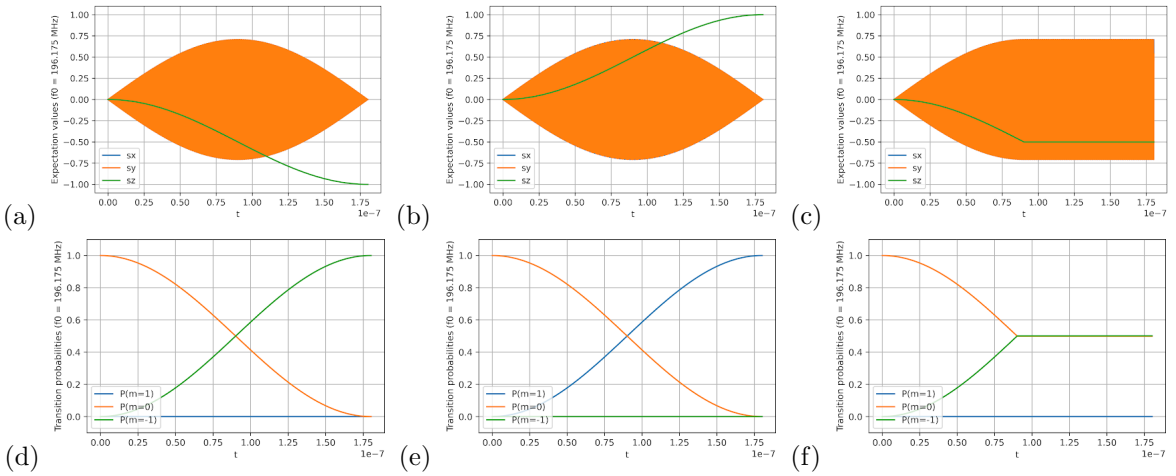


Fig. 3: (a), (b) & (c) show the transition-selective dynamics of the spin-1 NV-center under similar pulses as before, (d), (e) & (f) show the corresponding transition probabilities.

## 3 Simulating the Kicked-Top Hamiltonian

The Kicked-Top Hamiltonian is a simple dynamical system, Hamiltonian in character and capable of chaotic motion. It has a single degree of freedom and its two dimensional classical phase space is a sphere. Chaos is possible due to periodic driving, for simplicity chosen as a sequence of (delta function) kicks [4]. For the quantum description, we use the following Hamiltonian:

$$H_{KT}(t) = \alpha J_z + \frac{k}{2J} J_y^2 \sum_{n=-\infty}^{\infty} \tau\delta(t - n\tau) \tag{2}$$

where $J_z$ and $J_y$ are the (pseudo-)angular momentum operators in the 'z' and 'y' directions respectively and $J \equiv j + \frac{1}{2}$, setting $\hbar = 1$.

To capture the time evolution under this Hamiltonian, we set $\tau = 1$ and use the Floquet formalism to get the stroboscopic evolution equation:

$$|\psi(t)\rangle = U_\alpha(k) |\psi(t-1)\rangle = U_\alpha^t(k) |\psi(0)\rangle \tag{3}$$

where the unitary Floquet operator is,

$$U_\alpha(k) = e^{-ik\frac{J_y^2}{2J}} e^{-i\alpha J_z} \tag{4}$$

In principle, for chaos, we could apply the kicking to either the $J_z$ or the $J_y^2$ term, since the overall propagator remains unchanged. This will come in handy when we talk about the conditions for Non-linear metrology.
A standard lower-bound used in parameter estimation theory is derived from the Cramér-Rao inequality,

$$\delta^2\alpha \geq \frac{1}{I_\alpha(t)} \tag{5}$$

where $\alpha$ is the parameter to be estimated and $I_\alpha(t)$ is the Fisher Information.
As the Quantum Fisher information (QFI) is used to quantify a gradual separation between two quantum states that encode the same parameter $\alpha$ with a small difference $d\alpha$ between them, it is linked to the Bures distance, a distance measure between any two quantum states *rho* and *sigma*, given by

$$ds^2_{Bures}(\rho, \sigma) \equiv 2(1 - \sqrt{F(\rho, \sigma)}) \tag{6}$$

where $F(\rho, \sigma) = (\|\rho^{\frac{1}{2}}\sigma^{\frac{1}{2}}\|_1)^2$ is the fidelity and $\|A\|_1 \equiv tr\sqrt{AA^\dagger}$ denotes the trace norm. For pure states, $F(|\psi\rangle, |\phi\rangle) = |\langle\psi|\phi\rangle|^2$.
We now define the QFI as,

$$I_\alpha = 4ds^2_{Bures}(\rho_\alpha, \rho_{\alpha+d\alpha})/d\alpha^2 \tag{7}$$

To measure sensitivity to changes in the parameter, we use the Loschmidt echo technique, which measures the overlap $F_\epsilon(t)$ between a state propagated forward with a unitary operator $U_\alpha(t)$ and propagated backward with a slightly perturbed unitary operator $U_{\alpha+\epsilon}(-t) = U^\dagger_{\alpha+\epsilon}(t)$.

$$F_\epsilon(t) = |\langle\psi(0)| U_\alpha(t) U^\dagger_{\alpha+\epsilon}(t) |\psi(0)\rangle|^2 \tag{8}$$

This is the same fidelity that enters via the Bures distance in (7).
We benchmark the behaviour of the QFI using an initial SU(2)-coherent state given by,

$$|j, \theta, \phi\rangle = \sum_{m=-j}^{j} \sqrt{\begin{pmatrix} 2j \\ j-m \end{pmatrix}} \sin(\theta/2)^{(j-m)} \cos(\theta/2)^{(j+m)} e^{i(j-m)\phi} |jm\rangle \tag{9}$$

This state, without any kicking, gives a QFI:

$$I_\alpha(t) = 2t^2 j sin^2\theta \tag{10}$$

which is characteristic of the SQL-type of scaling. With a GHZ-state (also called the cat state) $(|j,j\rangle + |j,-j\rangle)/\sqrt{2}$, we get the trend,

$$I_\alpha(t) = 4t^2 j^2 \tag{11}$$

which shows the HL-type quadratic scaling in N ($N \equiv 2j$).
When we add the periodic delta-kicks, the characteristic Gaussian decay of the Loschmidt echo turns into a power law behaviour for small perturbations in $\alpha$. For $t_E < t < t_H$, where $t_E$ and $t_H$ are the Ehrenfest and Heisenberg time, $I_\alpha \propto tj^2$, corresponding to the HL-scaling, whereas for $t \gg t_H$, $I_\alpha \propto t^2 j$. This smooth transition can be observed in the plots generated here,

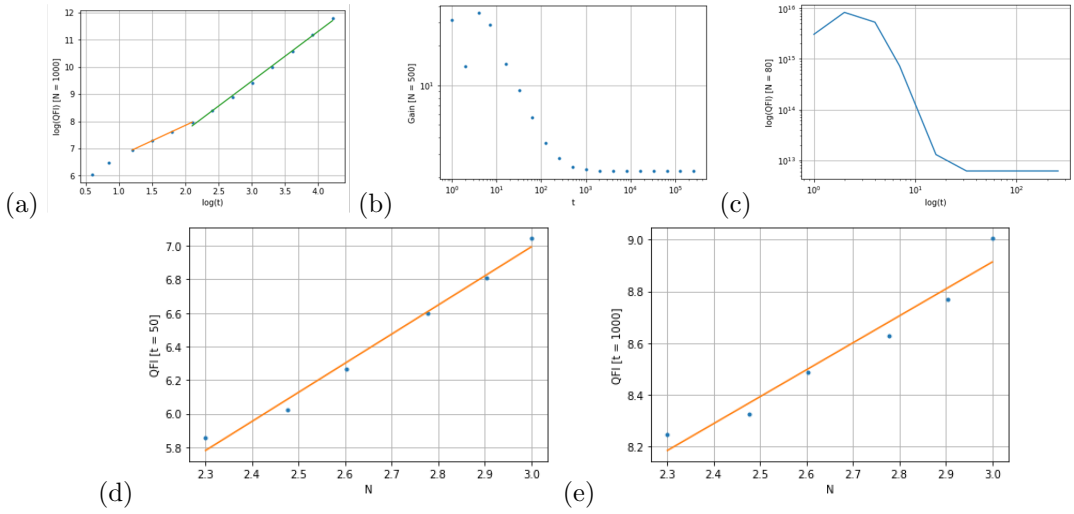


Fig. 4: (a) shows the smooth transition from the HL-scaling to SQL-scaling with respective linear fits having slopes as 1.1334 and 1.8334 respectively, (b) shows the gain in QFI as compared to the non-kicked coherent state evolution, where there is a clear gain up until the Heisenberg time when the scaling of the non-kicked top catches up with the kicked top, (c) shows the trend of QFI under the relevant T2 damping behaviour, (d) & (e) show the trend of QFI with N, with slopes of 1.735 for t=50 (HL-scaling) and 1.042 for t=1000 (SQL-scaling) respectively, and one can observe that these fall within the defined timescales under consideration. All plots take an initial coherent state with $(\theta, \phi) = (\pi/2, \pi/2)$ and fully chaotic Hamiltonians ($k = 30$)

## 4 Non-linear Metrology

Having established the results obtained for the KT Hamiltonian, we can see that there is promise to reach the Heisenberg limit without entangled state preparation. We now try to lay out a comparison with the generalised quantum single-parameter estimation using non-linear Hamiltonians and bring the KT Hamiltonian into this framework to observe the results.

## 4.1 Quantum Single-parameter Estimation

We consider a general Hamiltonian of the form,

$$H_\gamma(t) = \hbar\gamma h_0 + \tilde{H}(t), \quad h_0 = \sum_{\{j_1,\dots j_k\}} h^{(k)}_{j_1\dots j_k} \tag{12}$$

where $h_0$ is a dimensionless Hamiltonian that describes coupling to the parameter to be estimated and $\tilde{H}(t)$ is the auxilliary Hamiltonian that contains all *parameter-free* contributions to the Hamiltonian, including coupling to ancilla qubits for error-correction and other protocols. In $h_0$, $k$ denotes the degree of multi-body coupling, with the sum running over all subsets of $k$ systems. We assume that the $k$-body coupling $h^{(k)}$ is symmetric under exchange of probe systems. Moreover, we assume that $k$ and $h^{(k)}$ are independent of the number of probe systems.

Sergio Boixo et. al., in [1], used the symmetric logarithmic derivative-based definition of the QFI (which is shown to be equivalent to the Bures distance-based definition of the QFI in [2]) and defined a quantity called the operator semi-norm $\|H\|$ of an operator $H$, defined as $\|H\| = M_H - m_H$, where $M_H(m_H)$ is the maximum (minimum) eigenvalue of $H$. They then took the semi-norm of the generator of displacements in $\gamma$, $K_\gamma(t)$ and performed a chain of inequalities as mentioned below:

$$\frac{1}{\delta^2\gamma} \leq I_\gamma(t) \quad \text{(Cramér-Rao bound)} \tag{13}$$

$$I_\gamma(t) \leq 4\Delta^2 K_\gamma(t) \quad \text{(Equality for pure states)} \tag{14}$$

$$2\Delta K_\gamma(t) \leq \|K_\gamma(t)\| \quad \text{(By definition of semi-norm)} \tag{15}$$

$$\|K_\gamma(t)\| \leq t\|h_0\| \tag{16}$$

We get the last inequality by redefining $K_\gamma(t)$ in integral form and using triangle inequality and unitary invariance of semi-norm, as in [1]. It is important to note that this gives us an equality when $H_\gamma(t) = \hbar\gamma h_0$, and adding any auxilliary terms would only serve to equal or do worse than the case without them.
This finally yields,

$$\delta\gamma \geq \frac{1}{t\|h_0\|} \tag{17}$$

For a general Hamiltonian, this gives us a lower bound scaling of $\frac{1}{N^k}$, where $k$ is the degree of many-body coupling in the Hamiltonian. It is therefore clear that the auxilliary time-dependent part plays no role in deciding the overall lower-bound in this method and the deciding factor is $h_0$. One must keep in mind that even under the constraints set by the model, we are still free to choose the initial state and auxilliary term (although, as mentioned above, the auxilliary term can only serve to maintain $\|K_\gamma(t)\|$ or reduce it further).
It becomes difficult to compare the effect of initial entangled and separable states, as the many-body couplings themselves generate entanglement between the probes, so we resort to simulations to observe the differences.

## 4.2 KT Hamiltonian in Non-linear Metrology

As seen above, the crucial factor for deciding the scaling in the lower-bound is $\|h_0\|$.
To fit the the KT-Hamiltonian into this modelling, we must take the delta-kicking in the linear term (as mentioned, the kicking can equivalently be on either term) and the parameter to estimate is now

the coefficient $k$ of the non-linear term. Hence, $h_0$ becomes $\frac{J_y^2}{N+1}$, where $N = 2j$ is the number of probes, and

$$\|h_0\| = \begin{cases} \frac{1}{N+1} \times \left(\frac{N^2}{4}\right) & \text{if } N \text{ is even} \\ \frac{1}{N+1} \times \left(\frac{N^2-1}{4}\right) & \text{if } N \text{ is odd} \end{cases} \tag{18}$$

For large $N$, this gives us a scaling of $\frac{1}{N}$, despite the presence of non-linear terms.
One may think that the first recourse to this would be to eliminate the factor of $N + 1$ in the denominator from the Hamiltonian. The factor, however, is crucial to bridging the gap between the classical and quantum Hamiltonian in the limit of $N \to \infty$, so as to give equal weightage to the non-kicking and kicking terms. However, for the sake of completeness, we simulate both cases with and without the $N + 1$ factor.

## 4.3 Simulation Data

First, we will show simulations with $H_k = \frac{\hbar k J_y^2}{N+1}$ to affirm the bounds we derived in the previous subsection. The initial states taken as benchmarks for this are the SU(2) coherent state and the state $|\Psi_{ent}\rangle = \frac{1}{\sqrt{2}}(|M_{h_0}\rangle + |m_{h_0}\rangle)$. The latter is used instead of the cat state (as per the suggestion in the paper), since the assumption there is that the single-system operators have only non-negative eigenvalues, which is not the case in our system, so the state we've taken guarantees the equality condition as seen in the plots below:

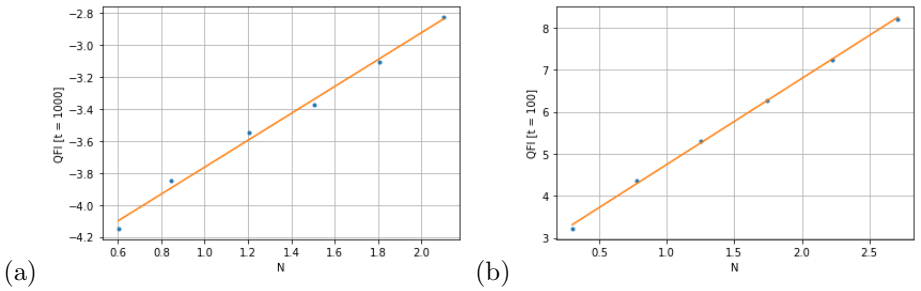


(a) (b)

Fig. 5: (a) & (b) show the trend for QFI with N for the initial SU(2)-coherent state and $|\Psi_{ent}\rangle$ respectively, with respective slopes of 0.897 (SQL) and 2.04 (HL).

When we remove the denominator of $N + 1$, as discussed, we observe the hypothesised scaling of $N^4$ for the QFI when the initial state is $|\Psi_{ent}\rangle$, in agreement with the model.

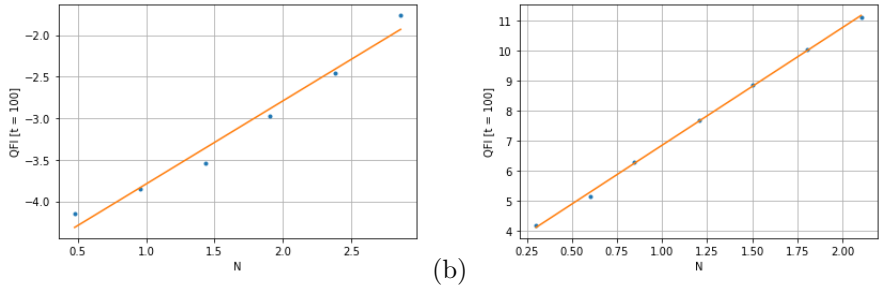


(a) (b)

Fig. 6: (a) & (b) show the trend for QFI with N for the initial SU(2)-coherent state and $|\Psi_{ent}\rangle$ respectively, with respective slopes of 0.998 (SQL) and 3.907 (beyond HL).

Introducing the linear kicking term to the non-linear term (without the denominator factor) and employing Floquet evolution, we see that with $|\Psi_{ent}\rangle$ as the initial state, there is a smooth transition from a higher than HL scaling upto a critical $N \sim 16$, beyond which it shows a higher than SQL trend.

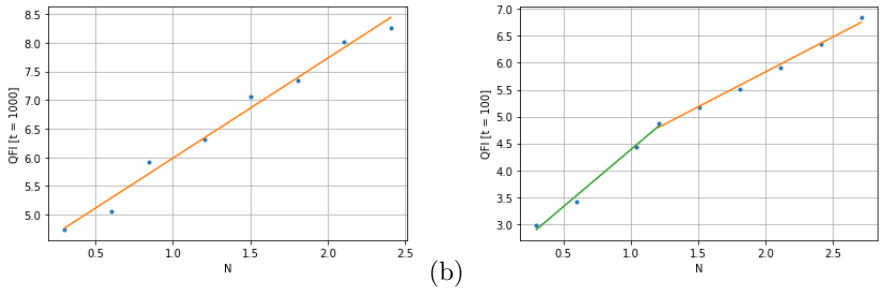


(a) (b)

Fig. 7: (a) shows the trend for QFI with N for the initial SU(2)-coherent state with slope of 1.746 (above SQL, below HL), and (b) shows that QFI scales with slope 2.124 (near HL) upto a critical $N \sim 16$, beyond which it scales with slope 1.302 (above SQL), with $|\Psi_{ent}\rangle$ as the initial state.

## 5 Conclusions

In this project, we have explored the avenues of numerically modelling the NV-center system's dynamics under resonance (with and without dissipation of different kinds), simulating the KT-Hamiltonian for a generalised spin ensemble and observing its behaviour at different timescales and system sizes, and finally exploring the connection between the KT-Hamiltonian and the Non-linear Metrology framework. Based on our calculations and simulation data, it is clear that Quantum Chaos can play a role in improving up until, but not beyond the Heisenberg limit on sensitivity. When taking away the denominator term, we can no longer look at the Hamiltonian as the quantum equivalent of the classical Kicked-top, but it does lend to scaling better than HL upto a critical $N$, as per the bound posited in [1], for a particular initial state. It is also interesting to note that there is a persistent scaling beyond SQL (but still limited by HL) for the initial coherent state even in this case, further indicating again that chaotic Hamiltonians show extra sensitivity to changes in the parameter as compared to integrable systems.

## References

[1] Sergio Boixo et al. "Generalized Limits for Single-Parameter Quantum Estimation". In: *Physical Review Letters* 98.9 (Feb. 2007). ISSN: 1079-7114. DOI: 10.1103/physrevlett.98.090401. URL: http://dx.doi.org/10.1103/PhysRevLett.98.090401.

[2] Samuel L. Braunstein and Carlton M. Caves. "Statistical distance and the geometry of quantum states". In: *Phys. Rev. Lett.* 72 (22 May 1994), pp. 3439–3443. DOI: 10.1103/PhysRevLett.72.3439. URL: https://link.aps.org/doi/10.1103/PhysRevLett.72.3439.

[3] Lukas J. Fiderer and Daniel Braun. "Quantum metrology with quantum-chaotic sensors". In: *Nature Communications* 9.1 (Apr. 2018). ISSN: 2041-1723. DOI: 10.1038/s41467-018-03623-z. URL: http://dx.doi.org/10.1038/s41467-018-03623-z.

[4] F. Haake and M. Kuś. "Kicked top". In: *Scholarpedia* 5.11 (2010). revision #137061, p. 10242. DOI: 10.4249/scholarpedia.10242.

[5] J.R. Johansson, P.D. Nation, and Franco Nori. "QuTiP: An open-source Python framework for the dynamics of open quantum systems". In: *Computer Physics Communications* 183 (8 2012), pp. 1760–1772. ISSN: 0010-4655. DOI: 10.1016/j.cpc.2012.02.021. URL: https://www.sciencedirect.com/science/article/pii/S0010465512000835.

[6] Romana Schirhagl et al. "Nitrogen-Vacancy Centers in Diamond: Nanoscale Sensors for Physics and Biology". In: *Annual Review of Physical Chemistry* 65.1 (2014). PMID: 24274702, pp. 83–105. DOI: 10.1146/annurev-physchem-040513-103659. eprint: https://doi.org/10.1146/annurev-physchem-040513-103659. URL: https://doi.org/10.1146/annurev-physchem-040513-103659.